Marine Geology, 96 (1991) 1–18
Elsevier Science Publishers B.V., Amsterdam

Acoustic measurements of suspended sand on the shoreface and the control of concentration by bed roughness

Christopher E. Vincent[a], Daniel M. Hanes[b]* and Anthony J. Bowen[c]

[a]*School of Environmental Sciences, University of East Anglia, Norwich NR4 7TJ, U.K.*
[b]*Rosenstiel School of Marine and Atmospheric Sciences, University of Miami, Miami FL 33149, U.S.A.*
[c]*Department of Oceanography, Dalhousie University, Halifax, N.S., Canada*

(Revision accepted July 3, 1990)

ABSTRACT

Vincent, C.E., Hanes, D.M. and Bowen, A.J., 1991. Acoustic measurements of suspended sand on the shoreface and the control of concentration by bed roughness. Mar. Geol., 96: 1–18.

Acoustic backscatter measurements of the concentrations of sand in suspension on the shoreface, seawards of the breaking zone, during a mild storm event show that sand concentrations increase initially but then rapidly decrease as the wave energy increases: it is suggested that the bed roughness is a major control on suspended sand concentration and that the decrease in concentration is due to decreasing ripple steepness after the break-off bed shear stress is exceeded. No direct measurements of bedforms were available and the combined wave-current interaction model of Grant and Madsen (J. Geophys. Res., Vols. 84 (1979) and 87 (1982)) with extensions to movable bed roughness (ripple dimensions from Carstens et al's. 1969 laboratory data (U.S. Army Corps Eng. CERC Tech. Mem. 28) and to sediment-induced self-stratification (Glenn and Grant, J. Geophys. Res., Vol. 92, 1983) was used to predict the current and suspended sand concentration profile. Matching the measured and modeled concentrations at 2 cm above the bed, the values of the resuspension coefficient γ_0 were found to decrease as excess skin friction increased, in a manner similar to that suggested by Drake and Cacchione (Cont. Shelf Res., Vol. 9, 1989) but were an order of magnitude larger. Using the much smaller ripple dimensions of Nielsen (J. Geophys. Res., Vol. 86, 1981) changed the model results very little. Significant differences were found between the time-averaged suspended sand profiles and those predicted by the model.

Sand transport fluxes have also been computed using the instantaneous products of measured suspended concentrations and currents (the current being the sum of steady and wave-induced components). The wave-induced fluxes show considerable variability from run to run but the general pattern is of a transport profile having a shoreward maximum at 5–10 cm above the bed and offshore transport in the few centimetres closest to the bed: little net transport occurred above 15 cm. These fluxes show a weak dependence on the wave energy, becoming more shoreware and the height of the maximum shoreward transport decreasing as the wave energy increased, again consistent with the influence of the ripple steepness.

1 Introduction

Most of us are familiar with the temporal changes which occur on beaches. Storms and other periods of high wave activity tend to move sand offshore; beach levels drop and the land behind the beach becomes more vulnerable to wave attack, to erosion or to flooding. During fair weather, often referred to as "summer wave conditions", a gradual accretion occurs and beach levels rise. These shorter term changes are often accompanied by more gradual changes in beach volume or position which may be due to alterations in sand supply to the beach (natural or man-induced) or to changes in the wave climate.

Such qualitative descriptions of how beaches alter mask the problems which exist in quantifying the processes which are responsible for such changes. The alongshore transport of sand driven by waves breaking on the shoreface at an angle can result in changes in beach levels if there is a

*Present address: Coastal and Oceanographic Engineering, University of Florida, Gainsville, FL 32611 (U.S.A.).

0025-3227/91/$03.50

flux divergence along the beach. However, most of the rapid changes in beach volumes are due to the cross-shore transport of sand; sand is transported from the upper beach face out to bars beyond the breaker zone and beach levels may be reduced by many tens of centimetres in the course of a single storm.

The data described here were collected as part of the C-COAST field experiment designed to investigate the hydrodynamic and sediment transport processes on beaches. The Canadian Coastal Sediment Transport Program (C-COAST) is a combined project of the Universities of Toronto, Dalhousie and Memorial and is sponsored by the National Science and Engineering Research Council of Canada. The results presented here are from a single acoustic concentration meter (ACM) and two electromagnetic current meters mounted close to the sea bed 100 m from the mean water mark during a field experiment on Queensland beach, Nova Scotia, during October 1987. Results from the other instrumentation recording concurrently will be presented elsewhere.

2 Queensland beach and the experimental design

Queensland beach is a small sandy pocket beach some 300 m wide, enclosed by rocky headlands. To the south it opens into a larger bay which itself opens to the Atlantic Ocean (Fig.1). Atlantic swell and storm waves penetrate through the bay opening, arriving as long-crested waves almost normal to the beach. The beach profile is a simple one with an upper shore face slope of 5° at mean water level (MWL), decreasing to 1.7° 100 m offshore (Fig.2). A surficial sand sample collected by divers 100 m offshore close to the ACM had a modal size of between 2.5 and 3.0ϕ when dry sieved through half-phi sieves (Fig.3).

Instrumentation, consisting of electromagnetic current meters, optical backscatter probes (OBS), acoustic concentration meters (ACM) and pressure sensors, was mounted on bottom frames 60, 70, 90 and 100 m from MWL (Fig.2). All were shore connected and, with the exception of the ACMs, the data were recorded on the Dalhousie University UDATS system (Hazen et al., 1988). Because of their high data return rate the ACMs recorded directly on their own PC-based logging systems. The ACM data presented here also recorded two "slow" channels of data taken from the UDATS system to ensure exact temporal sychronisation between the different logging systems.

The ACM was mounted 60 cm above the sea bed with its transducer axis vertical on the horizontal arm of an H-frame 100 m from MWL

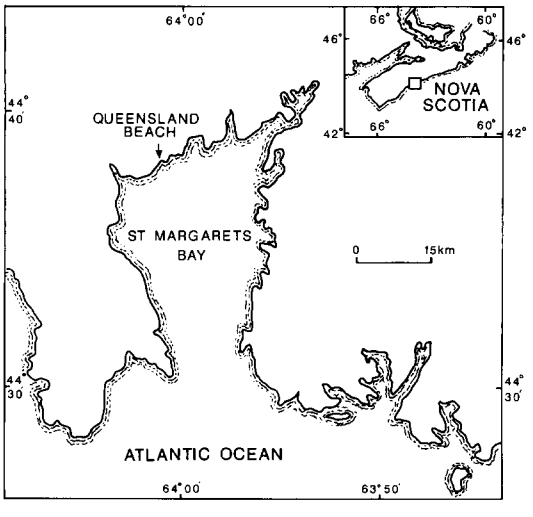

Fig.1. Location of Queensland beach, Nova Scotia.

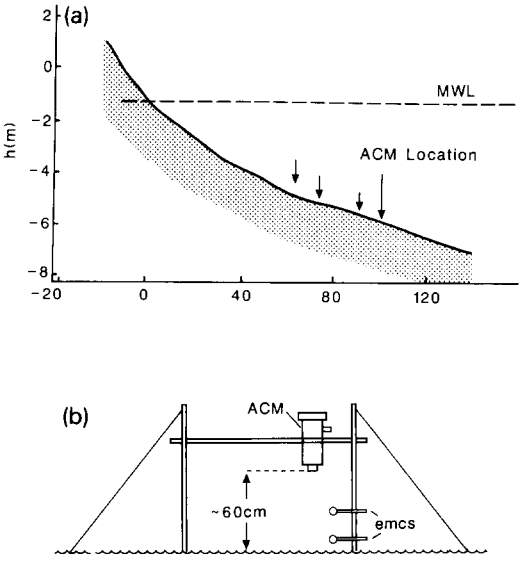

Fig.2. (a) Cross section of Queensland beach with the four major instrument locations. (b) H-frame with acoustic concentration meter (ACM) and electromagnetic current meters (EMCS).

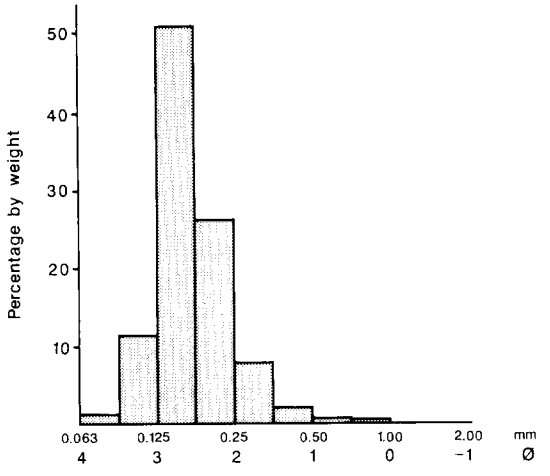

Fig.3. Sieved sand size distribution in half phi intervals of surficial sample taken from Queensland beach close to the ACM location.

(Fig.2). Current meters were fixed to one of the vertical arms of the frame at heights of 20 cm and 50 cm above the bed so that they measured the current close to the area ensonified by the ACM.

The instrumentation was positioned by divers who also made visual observations of bottom roughness and ripple wavelength whenever possible. A video camera was mounted near the 90 m frame and recordings made of resuspension events, but no direct information about ripple dimensions could be gathered for this storm due to poor visibility and low light levels.

3 The acoustic measurement of suspended sediment

3.1 The acoustic concentration meter

The acoustic concentration meter (ACM) used in this field experiment is similar to that described by Huff and Fiske (1980), Hanes et al. (1988) and Libicki et al. (1989). The acoustic frequency is 2.8 MHz and the pulse length is about 10 μs. Range gating the backscattered acoustic signal allows the sediment concentration profile to be estimated at 124 range "bins", with a vertical resolution of 0.81 cm. The pulse repetition rate was 10 Hz and four profiles were averaged before storing the data on disk together with two values from "slow" channels, on this occasion two components of an electromagnetic current meter. Disk access time and other software constraints meant that one average profile was recorded every 0.58 s. 1250 average profiles (12 min) were recorded during each run.

3.2 Calibration of the ACM

The ACM was calibrated in a laboratory recirculation tank (Vincent et al., 1986) using sand taken from the beach at Queensland. The calibration curves for sand at four concentrations are shown in Fig.4a, the digital value of the nominal voltage (8 bit, 0–255 scale) plotted against distance. The concentrations are those measured by withdrawing a water sample from the centre of the recirculation tank and then filtering and weighing the filtrate. These calibration profiles are each an average of 1250 individual profiles. The acoustic backscatter intensity V^2 (expressed here in terms of the notional voltage V seen by the system) from a uniform field of scatterers of concentration $C(r)$ is assumed to be an inverse function of range r with corrections for attenuation due to water and to the scatterers:

$$V^2 = Br^{-2}C(r)\exp\left\{-4\alpha r - \int_0^r \beta C(r)\,dr\right\} \qquad (1)$$

where B is a constant which includes the beam strength and sediment backscattering cross section, α is the attenuation due to water and β is the attenuation of the beam due to the presence of sediment. Here we assume a value of 1.1 dB/m for the absorption of 2.8 MHz sound by seawater and that β is 2.5×10^{-5} cm^{-1} (mg l^{-1})$^{-1}$ (Sheng and Hey, 1988). B depends on the acoustic power emitted by the transducer, the sediments in the water column and the gain of the receiver circuits. For this calibration (using Queensland sand) a value of 6.4×10^4 (mV^2 cm^2 mg^{-1} l) was found to fit the calibration data best. Normalising the backscattered acoustic energy using the above equation reduces the calibration data to that shown in Fig.4b: the region close to the transducer (5–25 cm) corresponds to the near-field region and fits the theoretical extent of the near field well (ka^2, where k is the acoustic wavenumber and a is the radius

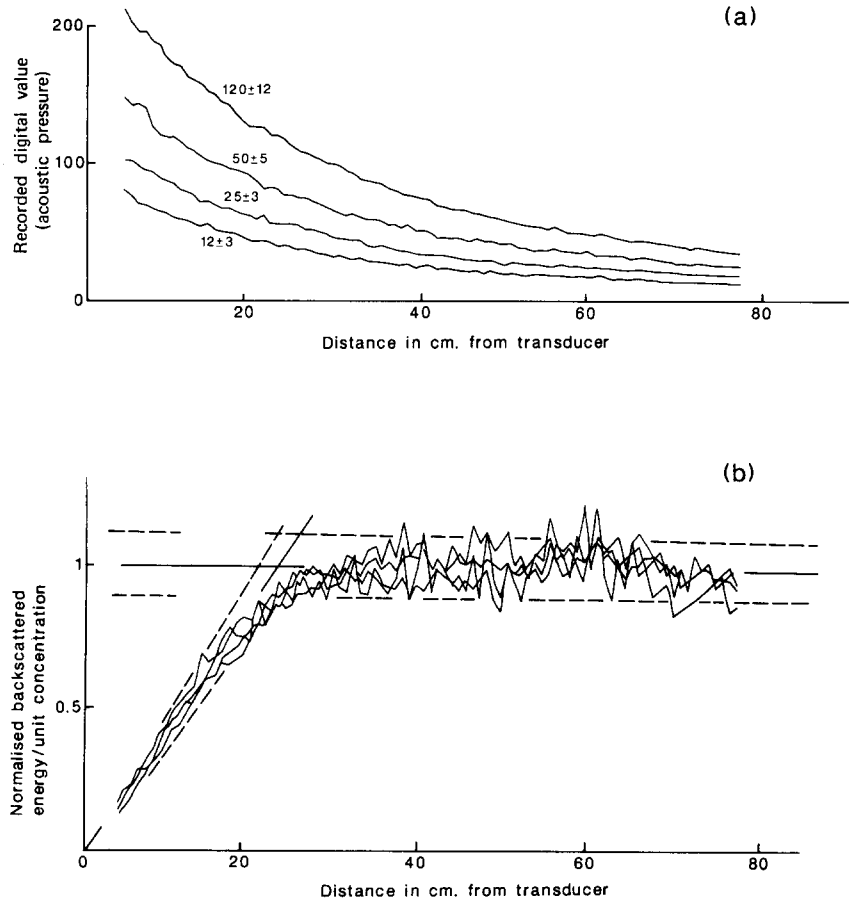

Fig.4. (a) Calibration curves for sand from Queensland beach in a recirculation tank for four concentrations. (b) Normalised backscatter signal intensities from the four calibration curves above. The near-field extends to 25 cm. Dashed lines are ±10% of the normalised value.

of the transducer). The field data are converted to concentrations using a step wise application of eqn. (10) with a linear correction in the near-field region as indicated in Fig.4b.

3.3 Limitations of the ACM

There are limitations to the effective use of the ACM for measuring rapid changes in the concentration of sediment above the sea bed (Vincent et al., 1986). Breaking waves inject bubbles into the water column and, as air bubbles have a high acoustic impedance, the ACM can clearly "see" them but it is difficult in any quantitative manner to differentiate between suspended sand and air bubbles; hence the ACM should not be used near the surf zone. At high suspended concentrations, difficulties can also be encountered because the acoustic beam is attenuated so rapidly that distance with little energy penetrates to the full range of the ACM; at 100 mg l^{-1} the attenuation is 0.6 db m^{-1} but provided high concentrations (> 1 g l^{-1}) are encountered only within a few centimetres of the sea bed, reasonable estimates of the concentration can still be made.

3.4 Sensitivity to particle size

Calibration tank tests with sieved sands suggest that an ACM operating at 2.8 MHz is most sensitive to sands between 1.0 and 1.5ϕ (0.5–0.35 mm). The calibration equation described

above assumes that the size distribution of the suspended sediment is always the same as that of the surficial sample collected. In the field the size distribution will vary both spatially and temporally so the calculation of the suspended concentration from the backscattered acoustic intensity may involve considerable uncertainty. The magnitude of this uncertainty cannot, therefore, be precisely quantified but for sand sizes which are much less than the wavelength of the sound (which is 0.58 mm at 2.8 MHz); halving the sand size halves the intensity of the backscattered signal.

3.5 Organic material in suspension

A further confusion in the interpretation of an ACM record was highlighted during a pre-storm trial of the instrumentation. Wave heights were very low (< 10 cm) and divers had reported that only occasional sediment suspension was occurring from the top of ripples on the sea bed. Visual monitoring of the ACM signal during this period showed clear and regular acoustic returns from the lowest 5 cm of the water column, returns which varied in intensity over a wave period as would be expected from sediment resuspension by waves. A further inspection of the sea bed beneath the ACM by one of the authors revealed that there was a layer of fine organic material floating close to the sea bed and being advected through the ACM beam by the wave motion. Spatial variations in the density and thickness of this organic material were seen by the ACM as a temporal variation in suspended concentration equivalent to a sand suspension of about 100 mg l^{-1} in the lowest 3–5 cm of the water column.

There is little that can be done to eliminate this problem as in many circumstances it will not be known if organic material is present in the water. During the deployment described below we expect the organic material to be dispersed more uniformly through the water column than in the situation described above. It should also be noted that a uniform suspension will appear as a signal in the transport due to the mean current but should integrate to zero for wave-induced transport, assuming the particles move with the water.

3.6 Accuracy and precision of the ACM measurements

Because of the likely variation in the sand size distribution with height above the sea bed it has not been possible to calculate the accuracy of the suspended sand concentrations: Vincent and Green (1990) show that the apparent concentrations above the sea bed under waves decreased faster than predicted by the Glenn and Grant (1983) model and suggested that this was due to finer material diffusing higher into the flow. During the Queensland experiment, suspended sand samples were taken at a number of heights above the botton near the 90 m size using a Nielsen suction sampler: there was some indication of a decrease in the model size of suspended sand but the differences were small (Greenwood, 1989, pers. commun.). The precision of the measurements is believed to be high and the calibration curves suggest a precision of $\pm 10\%$ in the assessment of the sand concentration, equivalent to the calibration sand size distribution.

4 Acoustic measurements of suspended sand concentrations during a mild storm event

4.1 Wave and current conditions

The event chosen for analysis was a 25 h period of onshore winds beginning at 0800 h on 28th October 1987 (Julian days 301–302). During this period, twenty 12 min runs of the ACM were recorded, of which sixteen had synchronous electromagnetic current meter (EMCM) data; runs are identified by Julian day plus a sequence number (301/1–301/13, 302/1–302/7). Examples of the temporal and spatial variations in the suspended sand concentrations during four runs (301/3, 301/11, 302/1 and 302/5) are shown in Fig.5 together with the EMCM current speeds. Mean currents, wave-induced currents and wave period for the complete period are summarised in Table 1.

Speeds from the shore-normal component of the EMCM at 20 cm above the bed (waves were approaching directly onto the shore) were used to calculate the wave-induced current and the wave period: no significant difference was found between the speeds measured by the EMCMS at

20 cm and 50 cm. Mean currents, speed and direction, were calculated from the two components of the EMCM at 20 cm. The method of analysis follows that used by Vincent and Green (1990). After subtracting the mean current, the wave period is found from the downward zero-crossing period. The maximum current is then found for each wave half-cycle and a "significant current" (defined in a similar way to the significant wave height, as the average of the highest one-third of the maximum currents) is identified for the onshore half-cycles and for the offshore half-cycles of the wave (Table 1).

4.2 Position of the sea bed

Suspended sand concentrations decrease rapidly away from the bed so an accurate assessment of

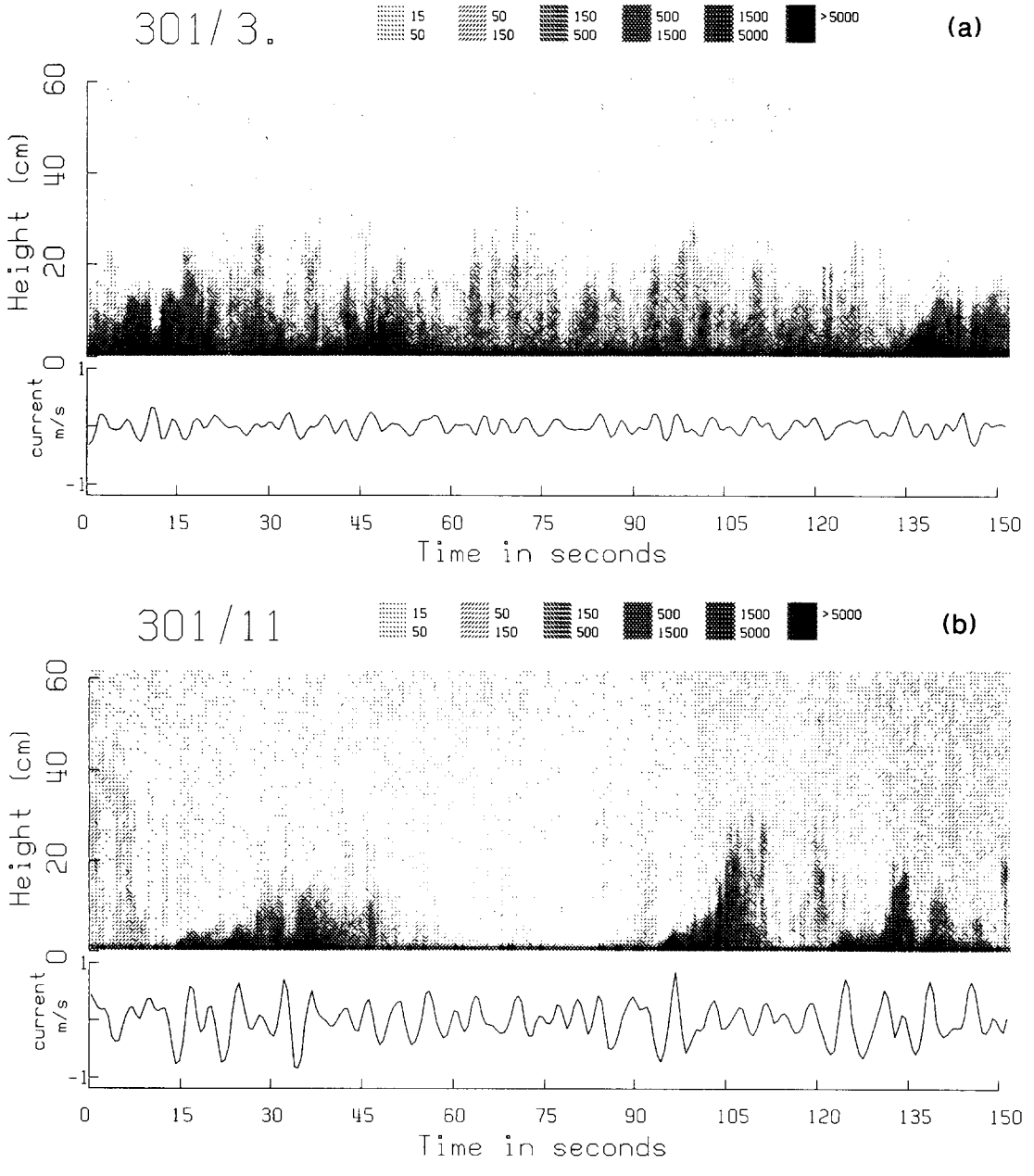

the position of the sea-bed is required. The level of maximum acoustic backscatter was interpreted as an echo from the sea bed: this level remained constant (± 1 bin, ± 0.8 cm) throughout each run, indicating that any bed features present were not moving significantly during that time, or that the amplitude of the bedforms was small (~ 1 cm). The acoustic footprint of the ACM is about 3.5 cm at the 60 cm range (defined by the position of the -20 db intensity contour of the acoustic beam).

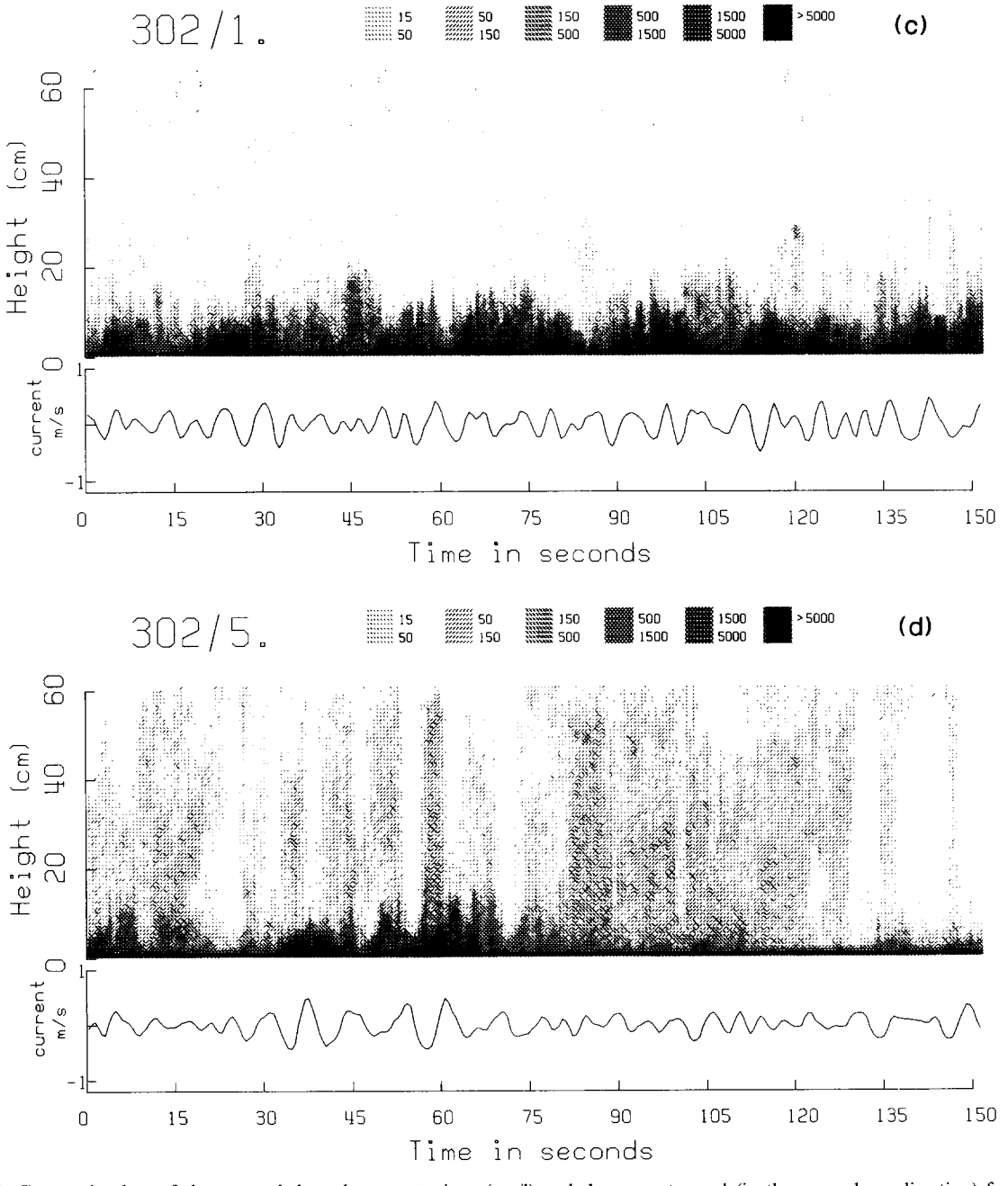

Fig.5. Grey-scale plots of the suspended sand concentrations (mg/l) and the current speed (in the cross-shore direction) for four bursts. (a) 301/3. (b) 301/11. (c) 302/1. (d) 302/5.

TABLE 1

Wave and current conditions during the 24 h mild storm event, showing the mean currents and the significant (sig) and average (av) wave-induced maximum currents for the onshore and offshore half-cycles (in cm s^{-1}). Bursts for which sychronous current data were not available are shown with asterisks

Burst No.	Time (h)	Mean currents (cm s^{-1})		Wave-induced currents				Wave period (s)
		On/off	Along	Onshore		Offshore		
				sig	av	sig	av	
301/1*	0815	2.6	−1.1	25	16	−27	−16	4.70
301/2*	0900	2.6	−1.1	25	16	−27	−16	4.70
301/3	1100	2.3	−0.6	24	15	−24	−15	4.36
301/4*	1300	3.1	−1.6	30	19	−31	−19	4.60
301/5	1530	4.1	−1.9	39	26	−40	−25	4.73
301/6*	1645	4.1	−1.9	39	26	−39	−25	4.74
301/7	1730	5.8	−2.8	52	35	−52	−32	4.92
301/8	1830	4.8	−1.6	58	39	−56	−35	4.95
301/9	1930	7.5	−4.3	61	39	−55	−34	4.95
301/10	2030	9.1	−5.8	73	48	−67	−40	5.12
301/11	2130	6.8	−3.7	61	40	−57	−35	5.08
301/12	2200	6.0	−3.8	62	40	−58	−37	5.34
301/13	2330	5.7	−3.2	50	32	−47	−30	5.54
302/1	0130	4.2	−2.0	37	23	−37	−23	5.10
302/2	0230	2.8	0.5	43	25	−41	−23	5.85
302/3	0330	2.6	0.7	37	24	−36	−22	6.12
302/4	0530	2.3	1.2	40	26	−39	−25	6.30
302/5	0630	2.0	0.9	32	20	−30	−19	5.91
302/6	0730	2.7	1.2	37	25	−33	−21	6.40
302/7	0850	2.9	1.2	38	24	−34	−21	6.38

A time series of bed heights from the individual profiles of run 301/8 ($\Delta T = 0.58$ s) and profiles smoothed over ten pulses ($\Delta T = 5.8$ s) is shown in Fig.6.

Over the period of the storm event however, the run-average sea bed position varies over more than 4 cm (Fig.7) but it is not possible to conclude how much of this variation is due to local erosion or deposition, or to the position of bedforms relative to the acoustic beam axis.

4.3 Run-average suspended sand concentrations

The concentrations of sand in suspension vary rapidly from second to second, producing a picture of complex suspension events (Fig.5). Time averaging the concentration profiles over the period of a run showed an unexpected pattern of suspended

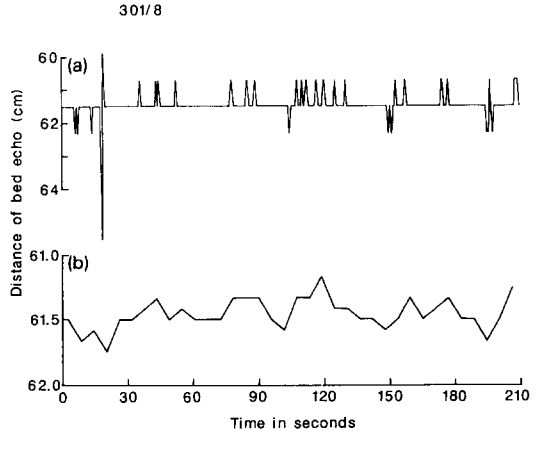

Fig.6. (a) Time series of the position of the sea bed, identified by the maximum echo strength for the first 210 s of burst 301/8 ($\Delta T = 0.58$ s). (b) Time series averaged over ten profiles ($\Delta T = 5.8$ s).

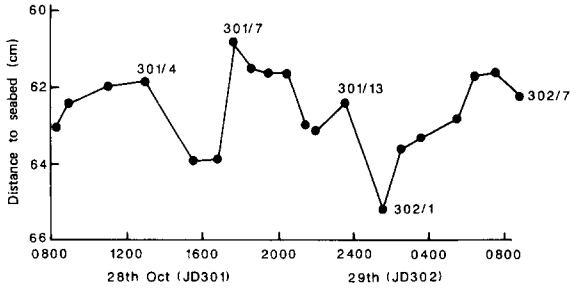

Fig.7. Burst-averaged positions of the sea bed over the period of the storm.

sand concentrations, with the lowest concentrations apparently associated with the period of highest waves (shown here by the largest wave-induced current speeds). A time series of run-averaged concentrations at four heights (2.5, 5, 12 and 25 cm) together with the wave-induced current speed and wave period is shown in Fig.8. There is a negative correlation, significant at 99%, between the significant wave orbital speed and concentrations at 2.5, 5 and 12 cm.

Three average run-mean profiles have been plotted in Fig.9 for periods when profile shape was not changing rapidly: the rising phase of the storm (301/1–301/4), the maximum wave height phase (301/7–301/12) and the waning phase (302/2–302/7). These average profiles differ from

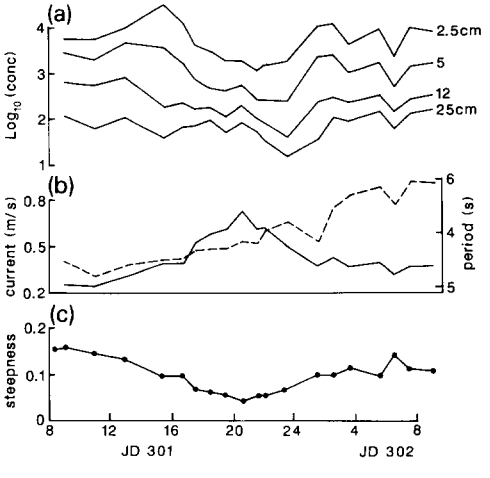

Fig.8. (a) Burst-averaged suspended sand concentrations at 2.5, 5, 12 and 25 cm above the sea bed (note the log scale). (b) Significant wave-induced currents (solid line) and the wave periods (dashed line). (c) ripple steepness from Carstens et al. (1969).

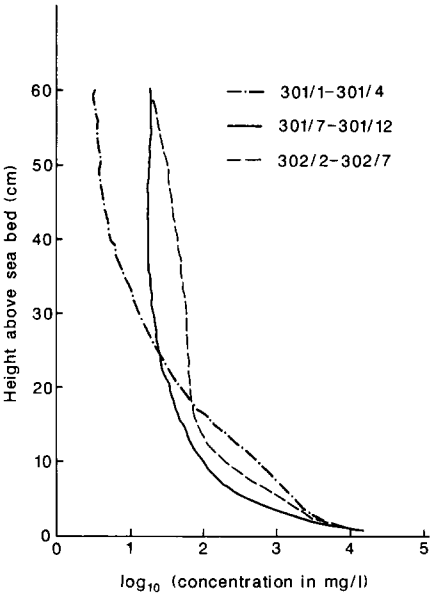

Fig.9. Average profiles for 301/1–301/3 (the rising storm), 301/6–301/11 (maximum wave heights) and 302/2–302/7 (the waning storm).

each other at most heights but the important differences are in the lowest 20 cm; above this level, much of the backscatter may be due to suspended organic material (see later).

5 Wave–current interaction, bed roughness and the resuspension of sand

Under a combination of a steady current and oscillatory flows, which are generated near the sea bed by surface waves, an interaction occurs between the waves and the currents. Close to the sea bed there is a shallow wave boundary layer while above this the steady current experiences an apparent roughness which is enhanced by the presence of the waves (Grant and Madsen, 1979). We have used the model developed by Grant and Madsen (1979, 1982) and Glenn and Grant (1983) for the wave–current interaction over a mobile bed, including the suspension of sand and a correction for any sediment-induced self-stratification which may occur (this model is henceforth referred to as the Grant–Madsen–Glenn or GMG model), to predict the combined flow characteristics and the bedforms. We have also compared the concentration measured 2 cm above the sea bed with that

predicted by the model. The model integrates the Smith and McLean (1977) expression for the reference concentration $C(z_0)$ over a wave period T:

$$C(z_0) = \frac{1}{T} C_b \int_{t=0}^{t=T} \frac{\gamma_0 S'(t)}{1 + \gamma_0 S'(t)} dt \quad (2)$$

where C_b is the bed volume concentration of sediment, γ_0 is an empirical constant, z_0 is the roughness height in the wave boundary layer and $S'(t)$ is the instantaneous normalised excess skin friction, defined as:

$$S'(t) = \frac{|\tau'(t)| - \tau_{cr}}{\tau_{cr}} \quad (3)$$

where $\tau'(t)$ is the instantaneous skin friction and τ_{cr} is the critical shear stress for initiation of motion. Various authors have suggested different values for γ_0 (Dyer, 1980; Wiberg and Smith, 1983; Hill et al., 1988; Vincent and Green, 1990) and recently Drake and Cacchione (1989) presented data which showed that γ_0 decreased rapidly as excess skin friction increased.

The steady current profile for non-stratified conditions applicable to all the data presented here, both within ($z < \delta_w$) and above ($z > \delta_w$) the wave boundary layer, is given by:

$$U(z) = (U^2_{*c}/\kappa U_{*cw}) \ln(z/z_0),\ z < \delta_w \quad (4)$$

$$U(z) = (U_{*c}/\kappa) \ln(z/z_{0c}),\ z > \delta_w \quad (5)$$

where $z_0 = k_b/30$ and k_b is the hydrodynamic roughness, and z_{0c} is the apparent roughness that retards the mean flow above the wave boundary layer. The friction velocity characteristic of $z > \delta_w$ is $U_{*c} = (|\tau_c|/\rho)^{0.5}$, where τ_c is the time-averaged instantaneous shear stress at the top of the boundary layer. $U_{*cw} = (|\tau_{cw}|/\rho)^{0.5}$ is the friction velocity applicable for $z < \delta_w$, where τ_{cw} is the maximum instantaneous boundary shear stress.

The neutral concentration profile is:

$$C(z) = C(z_0)\ (z/z_0)^{-\alpha},\ z < \delta_w \quad (6)$$

$$C(z) = C(\delta_w)\ (z/z_{0c})^{-\alpha},\ z > \delta_w \quad (7)$$

where α is the suspension parameter:

$$\alpha = \gamma w_f/\kappa U_{*cw} \text{ for } z < \delta_w \quad (8)$$

$$\alpha = \gamma w_f/\kappa U_{*c} \text{ for } z > \delta_w \quad (9)$$

w_f is the sand fall velocity and γ is an empirical constant set to 0.74 following Businger et al's. (1971) work in the atmospheric boundary layer.

The ripple geometry is defined empirically from the laboratory data of Carstens et al. (1969). The ratio of the maximum Shields parameter ψ' over a wave cycle to the critical Shields parameter ψ_c is used to define the break-off point where the ripple steepness begins to decrease:

$$(\psi'/\psi_c)_B = 1.8\ S_*^{1.6} \quad (10)$$

S_* is a dimensionless sediment parameter given by:

$$S_* = (D/4v)[(s-1)gD]^{0.5} \quad (11)$$

where v is the kinematic viscosity, s is the specific gravity of sand, g is the acceleration due to gravity and D is the sediment diameter. The Shields parameter is defined in the usual way as:

$$\psi = \tau/\rho(s-1)gD \quad (12)$$

where τ is the appropriate bed shear stress (the skin friction) and ρ is the density of seawater. The ripple heights η (from table 1 in Grant and Madsen, 1982) are given by:

$$\eta/a = 0.22\ (\psi'/\psi_c)^{-0.16} \text{ for } (\psi'/\psi_c) < (\psi'/\psi_c)_B \quad (13)$$

$$\eta/a = 0.48\ S_*^{0.8}\ (\psi'/\psi_c)^{-1.5} \text{ for } (\psi'/\psi_c) > (\psi'/\psi_c)_B \quad (14)$$

where a is the wave orbital excursion amplitude. The ripple lengths λ are:

$$\lambda/\eta = 6.25\ (\psi'/\psi_c)^{0.04} \text{ for } (\psi'/\psi_c) < (\psi'/\psi_c)_B \quad (15)$$

$$\lambda/\eta = 3.6\ S_*^{-0.6}\ (\psi'/\psi_c) \text{ for } (\psi'/\psi_c) > (\psi'/\psi_c)_B \quad (16)$$

We have run the GMG model using the wave and current data from the EMCMs; the onshore significant wave-induced current was used to represent the wave conditions in each run. The model was allowed to define its own equilibrium bedform conditions and to correct for any self-stratification (no significant sediment stratification was encountered during any of the runs presented here and all the results are effectively for neutral conditions). Table 2 shows the ripple height η, wavelength λ and steepness η/λ, the values of U_{*c}, U_{*cw}, z_{0c} and z_0 and the excess skin friction predicted by the model, the last term based on the assumption that

TABLE 2

Predicted bedforms, friction velocities and roughness lengths from the Grant–Madsen–Glenn model for each run, and the normalised excess bed friction

Burst No.	Bedforms			δ_w (cm)	U_{*c} (cm/s)	U_{*cw} (cm/s)	z_{0c} (cm)	z_0 (cm)	Normalised excess skin friction	γ_0
	η (cm)	λ (cm)	η/λ							
301/1	3.3	21	0.16	4.2	0.64	8.0	3.6	0.48		
301/2	3.3	21	0.16	4.2	0.64	8.0	3.6	0.48		
301/3	3.4	22	0.15	4.4	0.57	8.0	3.8	0.51	0.5	9.7
301/4	3.9	27	0.14	5.4	0.91	9.3	4.3	0.54		
301/5	2.6	28	0.093	5.2	1.05	8.6	3.6	0.25	2.4	4.6
301/6	2.6	28	0.093	5.2	1.05	8.6	3.6	0.25		
301/7	1.7	31	0.056	5.6	1.38	9.0	3.2	0.14	4.6	0.72
301/8	1.5	31	0.047	6.0	1.21	9.5	3.7	0.13	5.7	0.50
301/9	1.3	31	0.042	6.2	1.82	9.9	3.1	0.13	6.5	0.35
301/10	1.0	33	0.030	7.6	2.42	11.7	3.4	0.14	7.6	0.20
301/11	1.4	32	0.042	6.4	1.69	9.9	3.3	0.13	6.4	0.17
301/12	1.4	34	0.042	6.5	1.64	9.9	3.5	0.13	6.5	0.27
301/13	2.1	35	0.061	6.3	1.47	8.9	3.4	0.17	4.1	0.46
302/1	3.2	31	0.103	5.7	1.13	8.8	3.9	0.32	2.0	0.29
302/2	3.1	37	0.100	6.6	0.80	8.8	4.9	0.26	2.8	1.70
302/3	4.2	38	0.110	7.1	0.84	9.1	5.5	0.44	1.9	1.63
302/4	3.8	40	0.097	7.2	0.81	9.0	5.5	0.36	2.3	1.95
302/5	5.0	36	0.140	7.2	0.73	9.6	6.0	0.67	1.2	1.54
302/6	4.4	40	0.110	7.5	0.91	9.2	5.7	0.47	1.8	2.16
302/7	4.2	40	0.105	7.4	0.95	9.1	5.5	0.43	2.0	1.84

the average skin friction over ripples is the same as for that over a flat bed (Grant and Madsen, 1982).

5.1 *Variations in* γ_0

The values of γ_0 shown in Table 2 are the values required by the model to match the predicted suspended sand concentration at 2 cm above the sea bed with the measured values (average of concentrations from bins 2 and 3 above the bed). A reference concentration at 2 cm is preferred to that at 1 cm because of the uncertainty of ± 1 bin (± 0.8 cm) in the bed position; however, the strong concentration gradient near the bed will mean that $C(z_0)$ is very sensitive to the matching height chosen. The variation in γ_0 with excess skin friction is shown in Fig.10: the trend is similar to that found by Drake and Cacchione (1989) but the

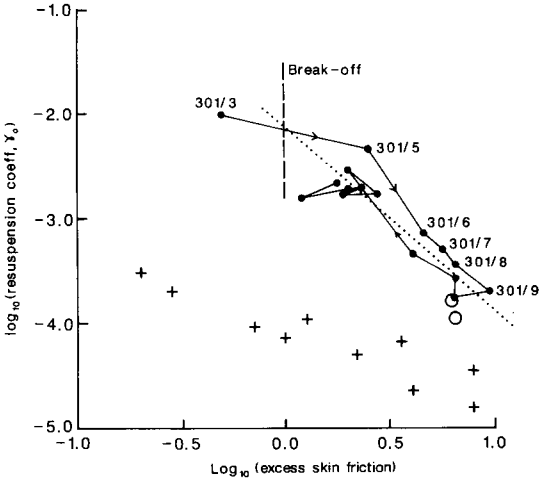

Fig.10. Plot of the variation in the resuspension coefficient γ_0 against the maximum (over one wave period) excess skin friction. ●This study; ○Vincent and Green (1990); +Drake and Caccione (1989).

values of γ_0 are generally an order of magnitude higher. Drake and Cacchione's values, however, were extrapolated from nephelometer data taken at a height of 1.9 m over a silt bed with a mean grain size of 16–25 μm. Towards the end of the storm period when wave heights were decreasing and bed roughness was greatest, the values of γ_0 were close to the value of 2×10^{-3} found by Smith and McLean (1977) in the Columbia River. During the higher excess skin friction period the values were very close to those measured by Vincent and Green (1990) for resuspension on a beach with similar-sized sand.

5.2 Comparison of modelled and observed concentration profiles

There are important differences, similar to those noted by Vincent and Green (1990), between the average concentration profiles and the concentration profiles predicted by the GMG model (Fig.11). In particular, the observed gradients of suspended sand are steepest close to the bed (in the wave boundary layer), whereas the model predicts a much more uniform gradient close to the bed. Also, it is difficuilt to identify any position as the top of the wave boundary layer in the observed profiles.

While these fundamental differences in the profile shapes show that the GMG model does not satisfactorily predict the average naturally occurring sand concentration profiles in this nearshore environment, the model's shortcomings are not unexpected. The GMG model is a two-layer model with the vertical eddy diffusivity being time-invariant and linear with height: it uses a single wave height, wave period, ripple height and ripple length. A real sea has a spectrum of wave heights and periods so the height of the wave boundary layer will vary from wave to wave, the ripples too are likely to be responding dynamically to the changing wave characteristics and vortex ejection *per se* cannot be considered because of the form of the eddy diffusivity profile. The differences do nevertheless warn of problems in using the GMG model to predict suspended sand concentration profiles.

6 On–offshore suspended transport rates

The transport of sand can be divided into two components, an advective term and a wave oscillatory term. The advective component of transport is due to the steady (time-averaged) current $\bar{U}(z)$ and the entire suspension of sand in the water is bodily transported. In the wave oscillatory component, where the net transport of water is by definition zero, sand transport occurs due to time lags between fluctuations in the current $U_w(z,t)$ and fluctuations in suspended sand concentrations $C(z,t)$. While the instantaneous current can be divided easily into steady and wave oscillatory components, $U(z,t) = U_w(z,t) + \bar{U}(z)$, it should be noted that the same cannot be done for the suspended sand concentration in any meaningful way: the sand concentration at any instant is due to the

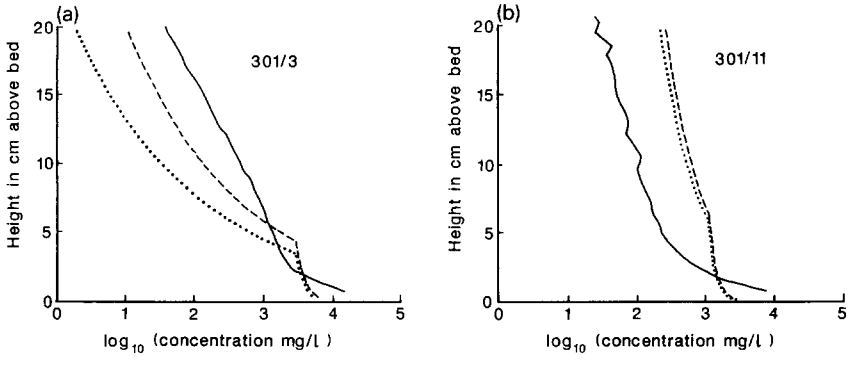

Fig.11. Comparison between the measured burst-averaged concentration profiles (solid lines) and those predicted using the GMG model with ripple dimensions determined from Carstens et al. (1969) (dashed lines) and from Nielsen (1981) (dotted lines) for bursts 301/3 and 301/11.

excess skin friction due to both waves and currents (alongshore as well as on–offshore) over a mobile bed formed by the combined system. Nevertheless, it is useful to compute the relative importance of the two components, as defined below.

The on–offshore component of the transport of suspended sand, averaged over the period of a burst, has been calculated in several ways, as follows:

(1) For steady currents, as a function of height above the bed ($Q(z)_{\text{mean}}$) and integrated over the water column (Q_{mean}):

$$Q(z)_{\text{mean}} = \bar{U}(z)\ \bar{C}(z) \tag{17}$$

and

$$Q_{\text{mean}} = \sum_{z=\text{sea bed}}^{z=60\text{ cm}} Q(z)_{\text{mean}} \tag{18}$$

where $\bar{C}(z)$ is the burst-mean concentration profile.

(2) For the wave oscillatory currents, again as a function of height from the bed ($Q(z)_{\text{wave}}$) and integrated over the water column (Q_{wave}):

$$Q(z)_{\text{wave}} = \sum_{t=0}^{t=\text{burst}} \overline{u_w(z,t)C(z,t)} \tag{19}$$

and

$$Q_{\text{wave}} = \sum_{z=\text{sea bed}}^{z=60\text{ cm}} Q(z)_{\text{wave}} \tag{20}$$

The average velocity profile was that predicted by the GMG model with neutral stratification matched with the measured currents at 20 cm. This also assumes that the current measured at 20 cm is in the potential flow region. Closer to the bed in the wave boundary layer, the current velocity at height z is given by:

$$U_w(z,t) = \left(1 - \frac{ker\,2\sqrt{\xi} + i\,kei\,2\sqrt{\xi}}{ker\,2\sqrt{\xi_0} + i\,kei\,2\sqrt{\xi_0}}\right) \times U_w(\infty, t) \tag{21}$$

where $U_w(\infty,t)$ is the wave-induced current outside the wave boundary layer, $\xi_0 = z_0/l$ and $\xi = z/l$ where $l = \kappa|U_{*cw}|T/\pi$, and *ker* and *kei* are Kelvin functions of the first order (Grant and Madsen, 1978). This equation shows the phase of the current changing towards the sea bed: the magnitude of this change is about 20° at 1 cm, less than the time resolution of the measurements (0.58 Hz) for most waves, so no attempt was made to correct for phase shift in these results.

6.1 *Vertically integrated transport*

The vertically integrated values of Q_{mean} and Q_{wave}, which describe the total sand transport (flux) past the measurement position, divided into the two components described above, are shown in Fig.12. The steady currents have an offshore component throughout the experimental period so the transport due to the steady current Q_{mean} is offshore throughout. The transport due to the wave oscillatory term Q_{wave} is of a similar magnitude to Q_{mean} but is generally directed towards the shore; the uncertainty limits shown are those which would result from an error of ± 1 bin in selecting the position of the sea bed. There is considerable variability in the transport flux from run to run although the general trend is for the flux to become

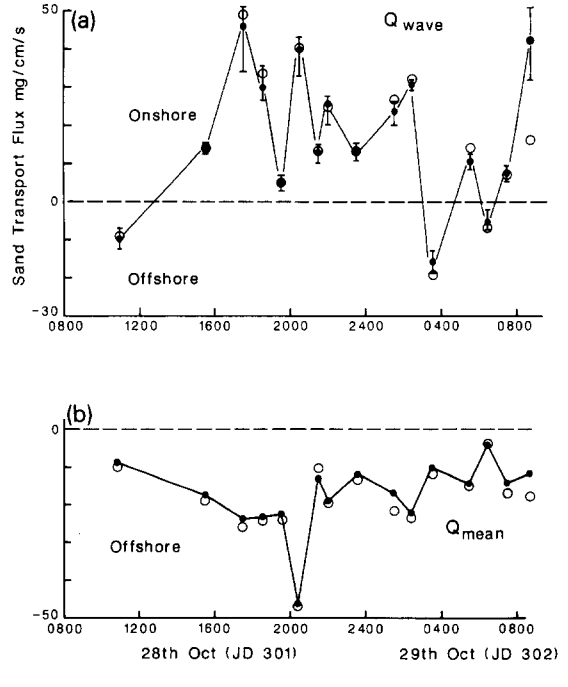

Fig.12. Vertically integrated values of the cross-shore sand transport due to the steady current (Q_{mean}) and to the waves (Q_{waves}) using the GMG model with ripple dimensions from Carstens et al. (1969) (●) and from Nielsen (1981) (○). The range of Q_{wave} shown on the Carstens values are those for an uncertainty of ± 1 bin.

more negative (shorewards) with the larger waves. The variability results partly from the flux being the resultant of large transports in opposite directions (gross transport is an order of magnitude larger than the net transport) but also from the groupiness of the waves; the influence of groupiness can be seen in Table 3 where the on–offshore flux has been calculated for each third of run 302/2.

6.2 *Transport profiles*

For each run the vertical profiles of suspended sand $Q(z)_{wave}$, $Q(z)_{mean}$ and the total transport $Q(z)_{total}$ in the on-offshore direction have been computed. Marked changes occur during the course of the storm, particularly in the heights at which maximum wave transport $Q(z)_{wave}$ is observed. With the exception of the last three runs (302/4–302/7), very little wave-induced transport occurs above 20 cm: the steady transport above 20 cm observed in a number of runs is probably due to contamination of the backscattered signal by suspended organic material. Figure 13 shows a sequence of suspended transport profiles from every other run for the lowest 20 cm. The wave component $Q(z)_{wave}$ (cross-hatched for clarity) is shorewards for all except the first profile (run 301/3), and has a peak transport elevation which decreases with height as the waves increase in height. During the final four runs (302/4–302/7) transport occurs to a much greater height from the bed ($\sim$50 cm), although still decreasing with height: this may be due to the efficient ejection of vortices from the ripple crests (predicted to be steep at this time) or perhaps to patchy organic material in suspension (see Fig.5d).

6.3 *Sensitivity of the transport estimates*

The sand transport values computed here clearly depend on the form of the current profile (both wave-induced and the steady component) chosen to occur below the EMCM at 20 cm. All the above results use the GMG model which includes ripple dimensions based mainly on laboratory experiments by Carstens et al. (1969). However, Nielsen (1981) noted that natural ripples, while obeying essentially the same rules as laboratory ripples, were shorter and less steep due to the irregularity of natural waves (Fig.14). To investigate the sensitivity of the results presented hitherto to the exact form of the current below 20 cm we have tried a number of forms for the profile, based on both the GMG model generating its own ripple dimensions (Carstens et al., 1969) and also on the model run with ripples defined from Nielsen (1981) for irregular waves alone:

$$\lambda/a = \exp \frac{693 - 0.37 \ln^8 M}{1000 + 0.75 \ln^7 M}$$

$$\eta/a = 21\, M^{-1.85}$$

where a is the wave semi-excursion and M is a mobility number defined as

$$M = (a\omega)^2/(s-1)gD$$

TABLE 3

Variation in the gross and net vertically integrated sand flux due to the waves during run 302/2 (values in parentheses are ranges). Three 240 s long segments, their wave-induced current speed and period are shown together with values for the complete run

Time period (s)	Wave current (cm/s)			On–offshore flux (mg/cm/s)	
	Onshore	Offshore	Period	Gross	Net
0–240	30	33	5.2	170 (19)	23 (25)
241–480	44	40	6.0	503 (47)	48 (49)
481–720	51	46	6.7	650 (84)	91 (89)
0–720	43	40	5.8	442 (49)	52 (55)

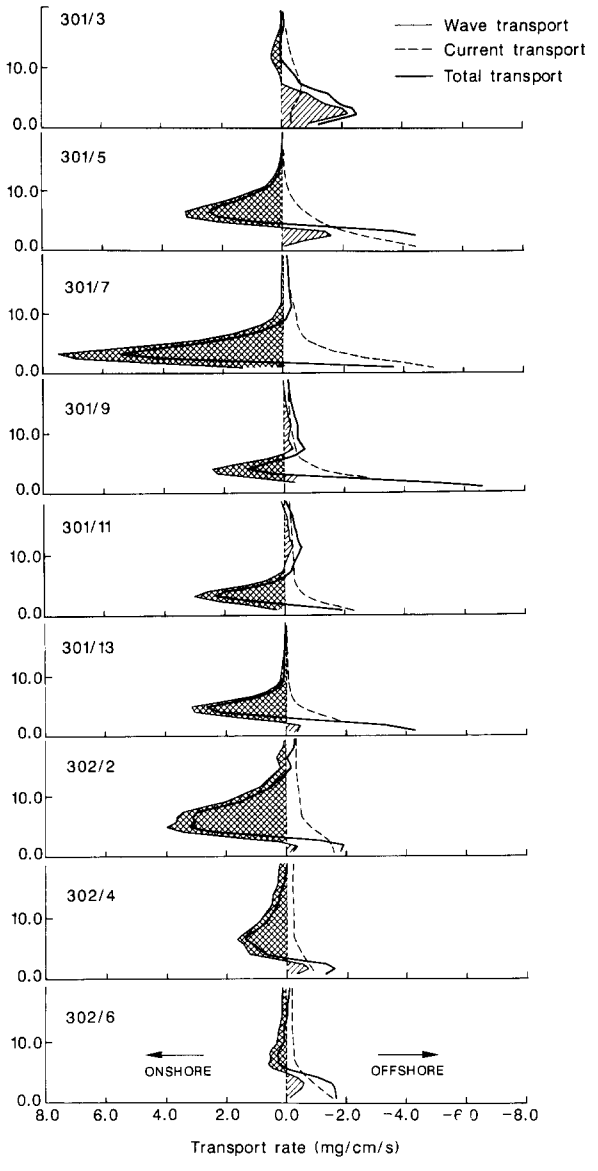

Fig.13. Run-averaged suspended sand transport profiles for the lowest 20 cm (every other run) showing the components due to the steady current and to waves. The cross-hatched region is the shoreware transport due to waves while the diagonal hatching is the offshore transport.

where ω is the wave radian frequency. The transport calculations have been repeated for the four time series shown in Fig.5 using a variety of flow profiles and the results are shown in Table 4 for the crosshore component of the transport. Firstly, the GMG model was run with:

(1) self-adjusting bed topography (Carstens et al., 1969).

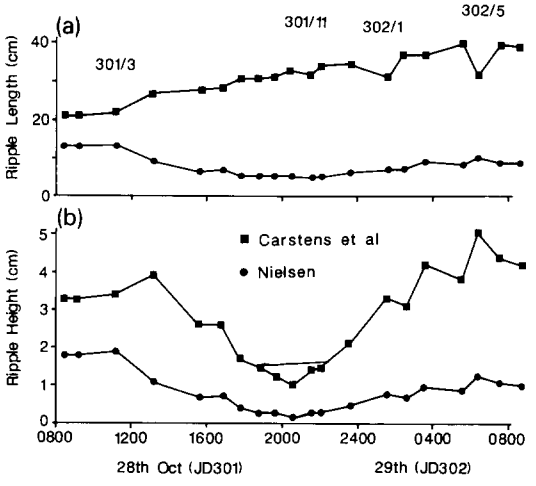

Fig.14. Comparison of the ripple height and length used by the GMG model for combined flow (based on Carstens et al., 1969), and those predicted by Nielsen (1981) for naturally occurring ripples under waves alone.

TABLE 4

The sensitivity of the vertically integrated burst-averaged transport computations to the assumptions about the form of the current profile. The variants (1) and (2) and (a) to (e) are defined in the text. Transport values are in mg/cm/s. For (c) to (e), shoreward transport is positive

		Q_{mean}		Q_{wave}		
		(a)	(b)	(c)	(d)	(e)
301/3	(1)	8.5	20.5	−8.2	−5.8	−11.0
	(2)	9.5	21.6	−9.7	−7.1	−11.0
301/11	(1)	13.0	20.5	13.2	5.2	15.5
	(2)	10.9	17.9	13.7	5.8	15.5
302/1	(1)	16.6	43.9	24.2	17.6	28.0
	(2)	22.1	52.1	26.7	17.6	28.0
302/5	(1)	3.5	9.3	−5.3	−3.0	−10.8
	(2)	4.7	11.1	−9.8	−4.7	−10.8

(2) GMG model with ripple dimensions from Nielsen (1981) using wave orbital data only (no currents) and then transport calculations made for the steady current Q_{mean} using

(a) the two-layer GMG flow profile, and

(b) a one-layer logarithmic profile defined by the measured current at 20 cm and K_b by the ripple height η.

The wave-induced transport Q_{wave} depends on the profile in the wave boundary layer. The following variants were used:

(c) current profile defined as in eqn.(11),

(d) wave-induced current decreases linearly from the top of the wave boundary layer to zero at the bed, and

(e) wave-induced current constant and equal to the velocity in the potential flow region.

Despite the large differences in the ripple dimensions predicted by the Carstens et al. (1969) laboratory data and Nielsen's (1981) field data, the difference between the transport rates (Table 4 (1) and (2)) is typically only 20%. The transport due the mean current Q_{mean} using the GMG two-layer model gives values which are about half those which are obtained if wave–current interaction is ignored and a simple logarithmic profile assumed (Table 4 (a) and (b)). With the highest sand concentrations occurring close to the bed the form of the wave-induced current profile close to the bed affects Q_{wave} significantly and is sensitive to the form wave profile. The profile (Table 4 (c)) based on the Grant and Madsen (1979) profile (eqn.11) is about mid-way between the results obtained by the linear model (d) and the constant model (e).

7 Discussion

No direct measurements or observations of the dimensions of the bedforms were available for this storm so it was necessary to estimate the amplitude and wavelength indirectly. While this is a severe limitation of the interpretation of the suspended sand data presented here there is sufficient consensus in the literature to suggest that, at wave conditions encountered during this storm, bedform steepness will decrease as wave heights increase.

Following the simple model for vortex shedding (Sleath, 1982) the vortex shed from the crest of a ripple by one wave half-cycle is swept upwards by the next (reversed) half-cycle. As the ripples decrease in steepness, this ejection becomes less efficient and sand is not lifted so high above the bed. At the final stage of an upper phase flat bed, no vortices will be formed and all the turbulence will be generated by the oscillatory flow over the sand grains resulting in a suspension remaining closer to the bed.

7.1 Parameterisation of the reference concentration

Quantitatively the changes in the reference concentration 2 cm above the bed are parameterised through the "constant" γ_0, but this is clearly inadequate for explaining the concentration observations shown in Fig.8. The average skin friction over a rippled bed in the Grant–Madsen–Glenn model is assumed to be equal to that which would occur over a flat bed with the same grain size: the variation in the total drag is assumed to be mainly due to changes in the form drag. These data indicate that there must be considerable variation in the skin friction, averaged over a ripple, compared with a flat bed. They are consistent with a high skin friction over the crests of ripples when the ripples are steep, before the break-off point (Grant and Madsen, 1982) is reached. Beyond break-off point, ripples decrease in steepness and the influence of ripple geometry in enhancing skin friction over the ripple crest decreases (such that the ripple-average skin friction also decreases) and less resuspension occurs.

A best-fit line through the data shown in Fig.10 gives the following relationship between γ_0 and the maximum excess shear stress S_{max} in a wave period:

$$\gamma_0 = 7.5 \times 10^{-3} S_{max}^{-1.8}$$

It is also noted that the values of γ_0 in Fig.10 show a suggestion of hysteresis, the higher values of γ_0 occurring when the waves are increasing in size and hence the ripples would tend to be steeper than their equilibrium value for the waves and sand suspension will be more than expected. As the waves decrease in height the reverse occurs, with ripples being lower and hence less sand would be suspended.

7.2 Transport profiles

Symmetrical waves over symmetrical ripples will result in no net sand transport. The transport profiles computed here, with their maximum wave-induced transport between 4 and 10 cm above the bed, result from flow (and hence bedform) asymmetry. The asymmetry of the wave motion alone is small, the peak currents below the wave crest being only a few centimetres per second faster than below the trough (Table 1); however, from consideration of waves alone the peak shear stress (and hence peak sediment resuspension) would occur beneath the wave crest. At Queensland beach the mean on–offshore current is of the order of 5 cm s^{-1} and is directed offshore (Table 1); this

current and the shear stress associated with it appears be sufficient to bias the peak bed stress towards the offshore wave half-cycle (although the shape of the mean current profile close to the bed is uncertain). With such a stress distribution, the time of maximum resuspension would occur under the wave trough (correlating with the tendency seen in Fig.3 for transport closest to the bed to be offshore) and ripples would have their asymmetry directed offshore. The shoreward flux from 5 to 15 cm is due to the half-cycle following the maximum stress sweeping the suspended sediment cloud upwards into the flow. The sand fall velocity of 2.3 cm s^{-1} and wave period of 5–6 s are consistent with maximum transport at the 5–10 cm height. The importance of the mean current to the direction of the wave-induced transport is also consistent with the transport profiles observed by Vincent and Green (1990) where the mean flow was shoreward and the wave-induced transport pattern was reversed (onshore close to the bed and offshore between 5 and 15 cm).

7.3 Time and space structure of suspension and bed roughness

The influence of the groupiness of waves on sediment resuspension has been noted by several authors (Clarke et al., 1982; Vincent et al., 1982) and can be seen in some of the suspension records (Fig.5). The variation in ripple geometry may help to explain this phenomenon. During the passage of a group of waves the sea bed will first be under the influence of small waves (generating steep ripples at equilibrium) and then under larger waves when ripples would be less steep (assuming the break-off point had been exceeded). A time lag would be expected in the response of the bed to the waves, so the big waves in the group would have a bed which was over-steep and which would efficiently eject sand-laden vortices high into the flow and, in the process, erode the ripple steepness. This vortex generation from ripples which are out of equilibrium (over-steep) may allow a series of high waves to advect the decaying vortices high into the water column. Conversely the smaller waves would experience a bed which was flatter than at equilibrium.

Figures 5b and c (301/3 and 301/11) show a good example of this process. From $t = 55$ s to $t = 85$ s in 301/11, virtually no resuspension occurs, yet in 301/3, where the wave-induced current speeds are about the same, resuspension is occurring with every wave and sand is lifted to 20 cm above the bed. We suggest that the difference is due to the more energetic waves prior to $t = 55$ s in 301/11 which have produced ripples of low steepness (approximately in equilibrium with the higher waves). In the low wave period which follows, no vortices can be ejected because of the low steepness and the ripples then start to build in steepness (initially as rolling grain ripples). When the next group of large waves arrives the ripples are over-steep once again and rapid vortex ejection and ripple erosion occurs.

8 Conclusions

Highlighted by these results is the importance of knowing the bed ripple dimensions during suspension events. Unfortunately, photographic techniques for ripple measurement, both video and stills, are very susceptible to any decrease in water clarity and a tracking high-frequency acoustic device is probably the best method for gaining suitable data during sand suspension events (Dingler and Clifton, 1984). Rapid profiling of the bed in the vicinity of the acoustic sand suspension measurements with a vertical resolution of a few millimetres would enable many points of speculation to be resolved, particularly those surrounding the variation in γ_0.

The major control on sand resuspension during groupy waves appears to be that of bed topography (ripple steepness) being out of equilibrium with the waves for most of the time, adding a further complication to the problem of modeling suspended sand transport. This also raises the question of the speed at which ripples respond to changing wave conditions; the groupiness of suspended transport suggests a time scale of a few wave periods but if the γ_0 values truly show hysteresis the time scale would be very much longer.

Whereas due to the variations in the distributions of sand sizes with height there must be

considerable uncertainty in the accuracy of translating the acoustic measurements into suspended sand concentrations, the points presented here should not be substantially altered because the assumption of a constant distribution should leave the results internally consistent. The measurement of the size distribution variations on time scales of an individual wave, perhaps through the use of multi-frequency acoustics, and its incorporation into the transport profiles must be considered as the next important step in understanding and predicting sand transport in the sea.

Acknowledgements

We wish to thank the very many members of the Universities of Toronto, Dalhousie, Memorial and East Anglia who took part in the Queensland beach experiment, without whom these data could never have been collected. C-COAST is supported by the National Science and Engineering Research Council of Canada. One of the authors (CEV) was supported by a grant from the Royal Society of London and one (DMH) by the U.S. Office of Naval Research.

References

Businger, J.A., Wyngard, J.C., Izumi, Y. and Bradley, E.F., 1971. Flux profile relationships in the atmospheric surface layer. J. Atmos. Sci., 28: 181–189.

Carstens, M.R., Neilson, R.M. and Altinbilek, H.D., 1969. Bedforms generated in the laboratory under oscillatory flow: analytical and experimental study. U.S. Army Corps Eng., Coastal Eng. Res. Cent., Tech. Mem. 28.

Clarke, T.L., Lesht, B., Young, R.A., Swift, D.J.P. and Freeland, G.L., 1982. Sediment resuspension by surface wave action: an examination of possible mechanisms. Mar. Geol., 49: 43–60.

Dingler, J.R. and Clifton, H.E., 1984. Tidal cycle changes in oscillation ripples on the inner part of an estuatine tidal flat. Mar. Geol., 60: 219–233.

Drake, D.E. and Cacchione, D.A., 1989. Estimates of the suspended sediment reference concentration (C_a) and resuspension coefficient (γ) from near-bed observations on the California shelf. Cont. Shelf Res., 9: 51–64.

Dyer, K.R., 1980. Current velocity profiles over a rippled bed and the threshold of movement of sand. Estuarine Coastal Mar. Sci., 10: 181–199.

Glenn, S.M. and Grant, W.D., 1983. A suspended sediment stratification correction for combined wave and current flows. J. Geophys. Res., 92: 8244–8264.

Grant, W.D. and Madsen, O.S., 1979. Combined wave and current interactions with a rough bottom. J. Geophys. Res., 84: 1797–1808.

Grant, W.D. and Madsen, O.S., 1982. Movable bed roughness in unsteady oscillatory flow. J. Geophys. Res. 87: 469–481.

Hazen, D.G., Huntley, D.A. and Bowen, A.J., 1988. UDATS: a system for measuring nearshore processes. Proc. Oceans '88, pp.993–997.

Hanes, D.M., Vincent, C.E., Huntley, D.A. and Clarke, T.L., 1988. Acoustic measurements of suspended sand concentrations in the C^2S^2 experiment at Stanhope Lane, Prince Edward Island. Mar. Geol., 81: 185–196.

Hill, P.S., Nowell, A.R.M. and Jumars, P.A., 1988. Flume evaluation of the relationship between suspended sediment concentration and excess boundary shear stress. J. Geophys. Res., 93: 12,499–12,509.

Huff, L. and Fiske, D.C., 1980. Development of two sediment transport instrument systems. Proc ASCE Conf. Coastal Eng., 17th, pp. 245–253.

Libicki, C., Bedford, K.W. and Lynch, J.F., 1989. The interpretation and evaluation of a 3 MHz acoustic backscatter device for measuring benthic boundary layer sediment dynamics. J. Acoust. Soc. Am., 85: 1501–1511.

Nielsen, P., 1981. Dynamics and geometry of wave-generated ripples. J. Geophys. Res., 86: 6467–6472.

Sheng, J. and Hay, A.E., 1988. An examination of the spherical scatterer approximation in aqueous suspensions of sand. J. Acoust. Soc. Am., 83: 598–610.

Sleath, J.F.A., 1982. The suspension of sand by waves. J. Hydraul. Res., 20: 439–452.

Smith, J.D. and McLean, S.R., 1977. Boundary layer adjustments to bottom topography and suspended sediments. In: J.C.J. Nihoul (Editor), Bottom Turbulence. Elsevier, New York, pp.123–152.

Vincent, C.E. and Green, M.O., 1990. Field measurements of the suspended sand concentration profiles and fluxes, and of the resuspension coefficient over a rippled bed. J. Geophys. R., 95: 15,591–15,601.

Vincent, C.E., Young, R.A. and Swift, D.J.P., 1982. On the relationship between bedload and suspended load transport on the inner shelf, Long Island, New York. J. Geophys. Res., 87: 4163–4170.

Vincent, C.E., Hanes, D.M., Tamura, T. and Clarke, T.L., 1986. The acoustic measurement of suspended sand in the surf-zone. Int. Conf. Measuring Techniques of Hydraulics Phenomena in Offshore, Coastal and Inland Waters. Br. Hydraul. Res. Assoc., London, pp.443–451.

Wiberg, P. and Smith, J.D., 1983. A comparison of field data and theoretical models for wave-current interactions at the bed on the continental shelf. Cont. Shelf Res. 2: 147–162.